Oncogenic stress sensitizes murine cancers to hypomorphic suppression of ATR

David W. Schoppy[1], Ryan L. Ragland[1], Oren Gilad[1], Nishita Shastri[1], Ashley A. Peters[1], Matilde Murga[2], Oscar Fernandez-Capetillo[2], J. Alan Diehl[1] and Eric J. Brown[1,3]

[1]Abramson Family Cancer Research Institute and the Department of Cancer Biology, Perelman School of Medicine, University of Pennsylvania, Philadelphia, PA

[2]Genomic Instability Group, Spanish National Cancer Research Centre (CNIO), Madrid, Spain

[3]To whom correspondence should be addressed:

Abramson Family Cancer Research Institute and the Department of Cancer Biology, Perelman School of Medicine, University of Pennsylvania, 514 BRB II/III, 421 Curie Boulevard, Philadelphia, PA 19104-6160

Phone: (215) 746-2805

Fax: (215) 573-2486

Email: brownej@mail.med.upenn.edu

Supplemental Figure 1

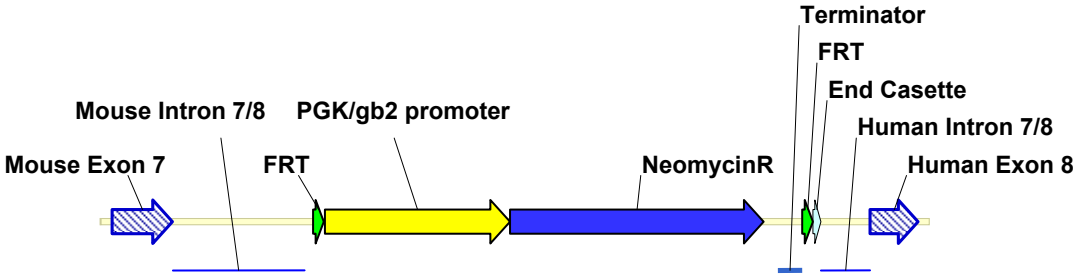

ATR^{seckel} sequence (2624 bp)

CCATAATGTCAAGGATCATCAACACAAATATAAGAAGAAACCTCCAGTAGTAGTAACTTGGATGTCT
TTGGATTTTTATACAAAAGTGCTTAAAAGCTGTAGGAGTTTGTTAGAATCTGTTCAGAAACTTGAACT
GGAATTAGTCATTGATAGCATGGTGAGAATTTGTGATGCTCTGATGTATATGCAAGgtgagtacaactaagtgat
agacgttagtcattgtagatgaaggctttctgtttctgtttcaagtttaaatgcagaagtactgttaatattcagaatattttcaatttttctgttaattaagcttactggtagtttctg
agtttcacatttacttgtatagcattttgatttggtcaatagacattcatttgaaacatttaaatgttttggtttgagaatctgaagaacactatgatccatatagatggtatatata
aatgcatatggttttaagccacatctgatttcactggcctcacagacttcagcatgggcctggaagtatagctcagtggtagaatacatgttaaatgtgtgcaaggtttgtca
cagatcactcccagttaaaacagaagattgtttcttgccctttgtttta|**aattaaccctcactaaagggcggccgcgaagttcctattctctagaaagtataggaactt**
cattctaccgggtaggggaggcgcttttcccaaggcagtctggagcatgcgctttagcagccccgctgggcacttggcgctacacaagtggcctctggcctcg
cacacattccacatccaccggtaggcgccaaccggctccgttctttggtggccccttcgcgccaccttccactcctccctagtcaggaagttcccccccgccc
cgcagctcgcgtcgtgcaggacgtgacaaatggaagtagcacgtctcactagtctcgtgcagatggacagcaccgctgagcaatggaagcgggtaggcctt
tggggcagcggccaatagcagctttgctccttcgctttctgggctcagaggctgggaaggggtgggtccgggggcgggctcaggggcgggctcaggggcg
gggcgggcgcccgaaggtcctccggaggcccggcattctgcacgcttcaaaagcgcacgtctgccgcgctgttctcctcttcctcatctccgggcctttcgacc
tgcagcagcacgtgttgacaattaatcatcggcatagtatatcggcatagtataatacgacaaggtgaggaactaaaccatgggatcggccattgaacaag
atggattgcacgcaggttctccggccgcttgggtggagaggctattcggctatgactgggcacaacagacgatcggctgctctgatgccgccgtgttccggct
gtcagcgcaggggcgcccggttctttttgtcaagaccgacctgtccggtgccctgaatgaactgcaggacgaggcagcgcggctatcgtggctggccacga
cgggcgttccttgcgcagctgtgctcgacgttgtcactgaagcgggaagggactggctgctattgggcgaagtgccggggcaggatctcctgtcatctcacct
tgctcctgccgagaaagtatccatcatggctgatgcaatgcggcggctgcatacgcttgatccggctacctgcccattcgaccaccaagcgaaacatcgcat
cgagcgagcacgtactcggatggaagccggtcttgtcgatcaggatgatctggacgaagagcatcaggggctcgcgccagccgaactgttcgccaggctc
aaggcgcgcatgcccgacggcgaggatctcgtcgtgacccatggcgatgcctgcttgccgaatatcatggtggaaaatggccgcttttctggattcatcgact
gtggccggctgggtgtggcggaccgctatcaggacatagcgttggctacccgtgatattgctgaagagcttggcggcgaatgggctgaccgcttcctcgtgct
ttacggtatcgccgctcccgattcgcagcgcatcgccttctatcgccttcttgacgagttcttctgagcgggactctggggttcgaataaagaccgaccaagcg
acgtctgagaggctcctggcgaattcggtaccaataaaagagctttattttcatgatctgtgtgttggtttttgtgtgcggcgcggaagttcctattctctagaaa
gtataggaacttcctcgagccctatagtgagtcgtatta|cccgggtcacagacctcagaccatcgtttatagatctctgtgttaagaatttctgcttatccaatgatcatt
atgatagtatttcaaatgtctttatttttatttaaaagagatatgattaaggaaaagttataattaatgacttattttgtgcttctgtagTAAACAGTTCATTTGAA
GATCATATCCTGGAAGATTTATGTGGTATGCTCTCACTTCCATGGATTTATTCCCATTCTGATGATGG
CTGTTTAAAGTTGACCACATTTGCCGCTAATCTTCTAACATTAAGCTGTAGGATTTCAGATAGCTATT

CAPS: exon sequence (mouse exon 7 and human exon 8)
Lower case: intron sequence (mouse or human)
Bold: Targeting Cassette (FRT-PGK-gb2-neo-FRT, GeneBridges), | = cassette boundaries
Highlighting: Green: FRT; Yellow: Promoter; Blue: Neomycin R; Purple: Neo forward & exon 8 reverse primers
Underlined: sequence confirmed by cloning and sequencing

Supplemental Figure 1. Illustration and sequence of 5' region of humanized ATR^{seckel} allele. (Top Panel) Illustration of 5' region humanized ATR^{seckel} allele with identification of relevant features. (Bottom Panel) Sequence of region represented in top panel. Sequence confirmed by cloning and sequencing is underlined.

Supplemental Figure 2

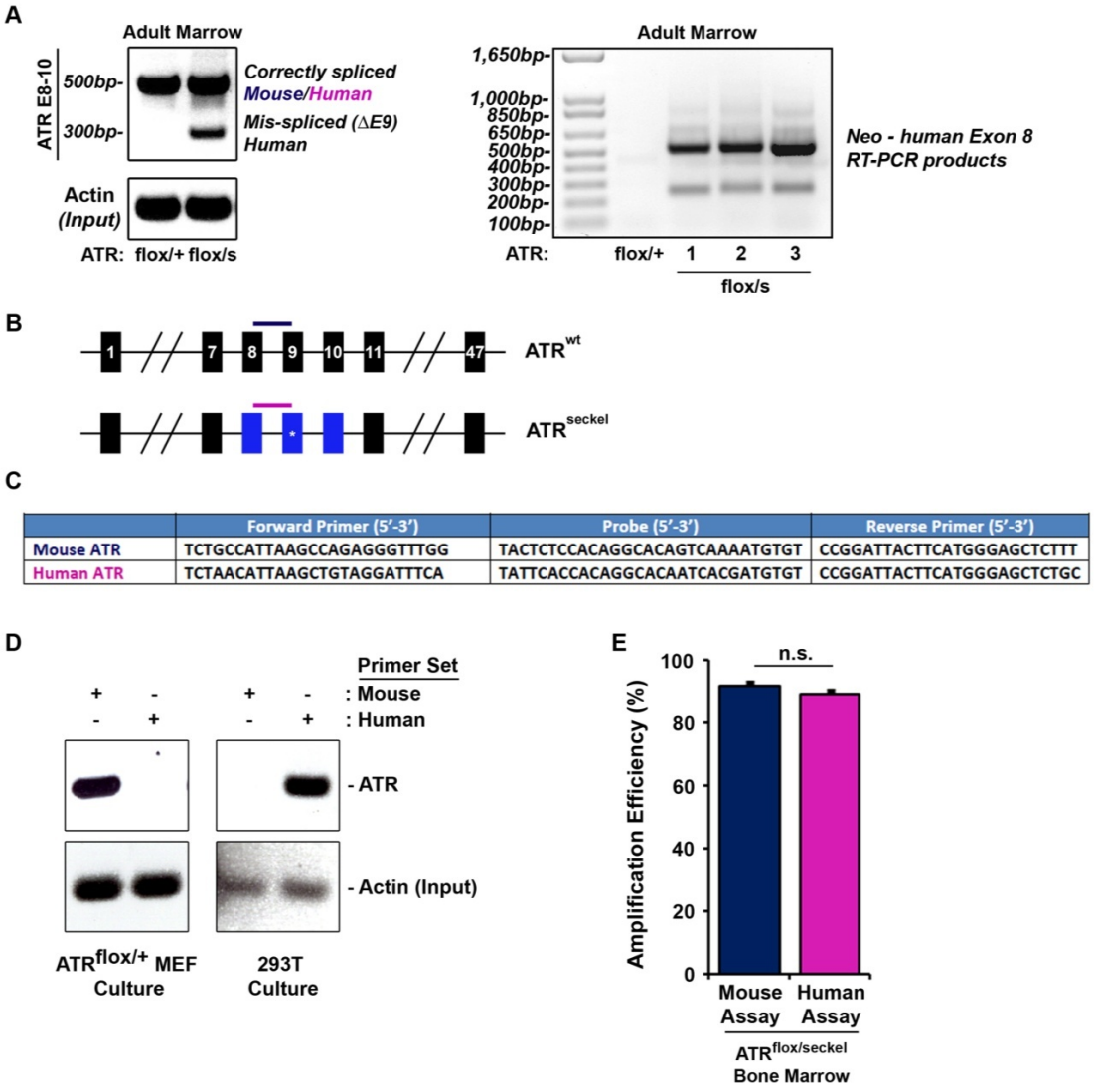

Supplemental Figure 2. Multiple ATR^{seckel} mRNA transcripts and a discriminating qRT-PCR assay to quantify the relative amount of correctly spliced mouse and human ATR in adult tissues. (**A**) PCR analysis of reverse transcribed RNA isolated from adult bone marrow using non-discriminating primers amplifying exons 8 to 10 of ATR (left panel) and primers amplifying the Neomycin resistance gene to exon 8 in three ATR$^{flox/seckel}$ mice (right panel). In ATR$^{flox/seckel}$ marrow, ATR containing exon 9 (500bp band) is contributed to by both mouse ATR (ATR^{flox}) and human ATR (ATR^{seckel}). Mis-spliced ATR lacking exon 9 (300bp band) can be observed below the band representing correctly spliced ATR (left panel). Several transcripts of varying lengths were observed using primers recognizing the Neomycin resistance gene and exon 8 (right panel). The ~550 bp band corresponds to non-terminated transcripts from the Neo cassette (primer binding sites shown in Figure 1). Splicing into and out of Neo-containing cassettes has been well documented (1-4). (**B**) Diagram of mouse ATR (ATR^{wt}, top) and 'humanized' Seckel ATR (bottom), depicting mouse exons (black boxes) and human exons (blue boxes), and the ATR^{seckel} mutation (*). The horizontal bars above each allele denote the binding location of the discriminating qRT-PCR assays (primer and probe sets) designed to recognize either correctly spliced mouse ATR (blue bar) or correctly spliced human ATR (pink bar). (**C**) Discriminating qRT-PCR assays as described in (B). (**D**) PCR analysis of RNA isolated from MEF cultures (left panels) or 293T cultures (right panels) using primers from **C**. The mouse PCR primer set amplifies mouse ATR but does not detect human ATR, while the human PCR primer set fails to detect mouse ATR but recognizes human ATR. (**E**) Assessment of the amplification efficiency of the qRT-PCR assays listed in **C**. Amplification efficiency was calculated from standard curve analysis of RNA isolated from adult bone marrow (n = 5) using the equation E (efficiency) = $(10^{-1/slope} - 1) \times 100$, as described in manufacturer's instructions (Applied Biosystems). The amplification of each assay did not differ significantly from the other and amplification efficiency of each assay was consistently ≥ 90% across a range of tissues and culture samples.

Supplemental Figure 3

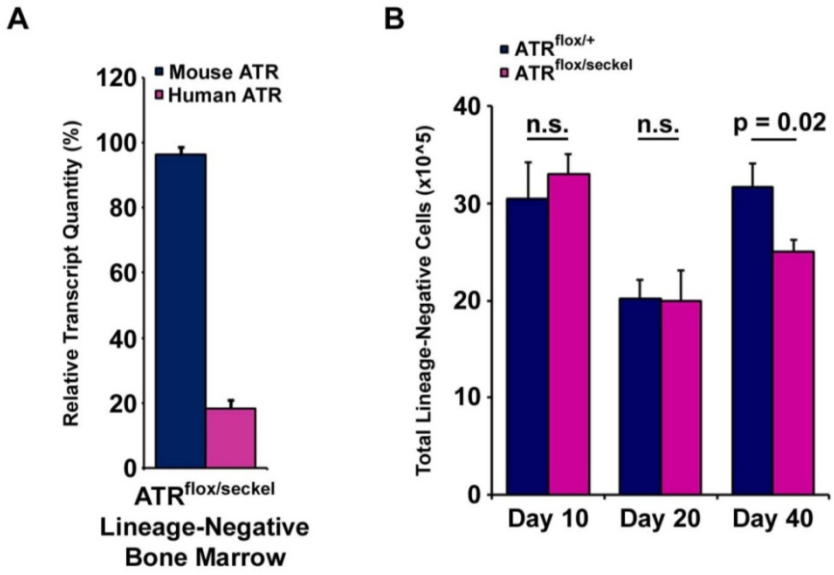

Supplemental Figure 3. ATR suppression has no appreciable effect on the representation of lineage-negative bone marrow progenitors. (**A**) Quantification of correctly-spliced mouse (ATR^{flox}) and human (ATR^{seckel}) ATR transcript in sorted adult (6-8 week-old) lineage-negative bone marrow (CD3-negative, B220-negative, Ter119-negative, Mac1-negative). (**B**) Absolute number of lineage-negative bone marrow cells (CD3-negative, B220-negative, Ter119-negative, Mac1-negative) obtained from 4 hindlimb bones of mice at the indicated time points after initial TAM treatment (n = 5-15 mice per genotype, per time point).

Supplemental Figure 4

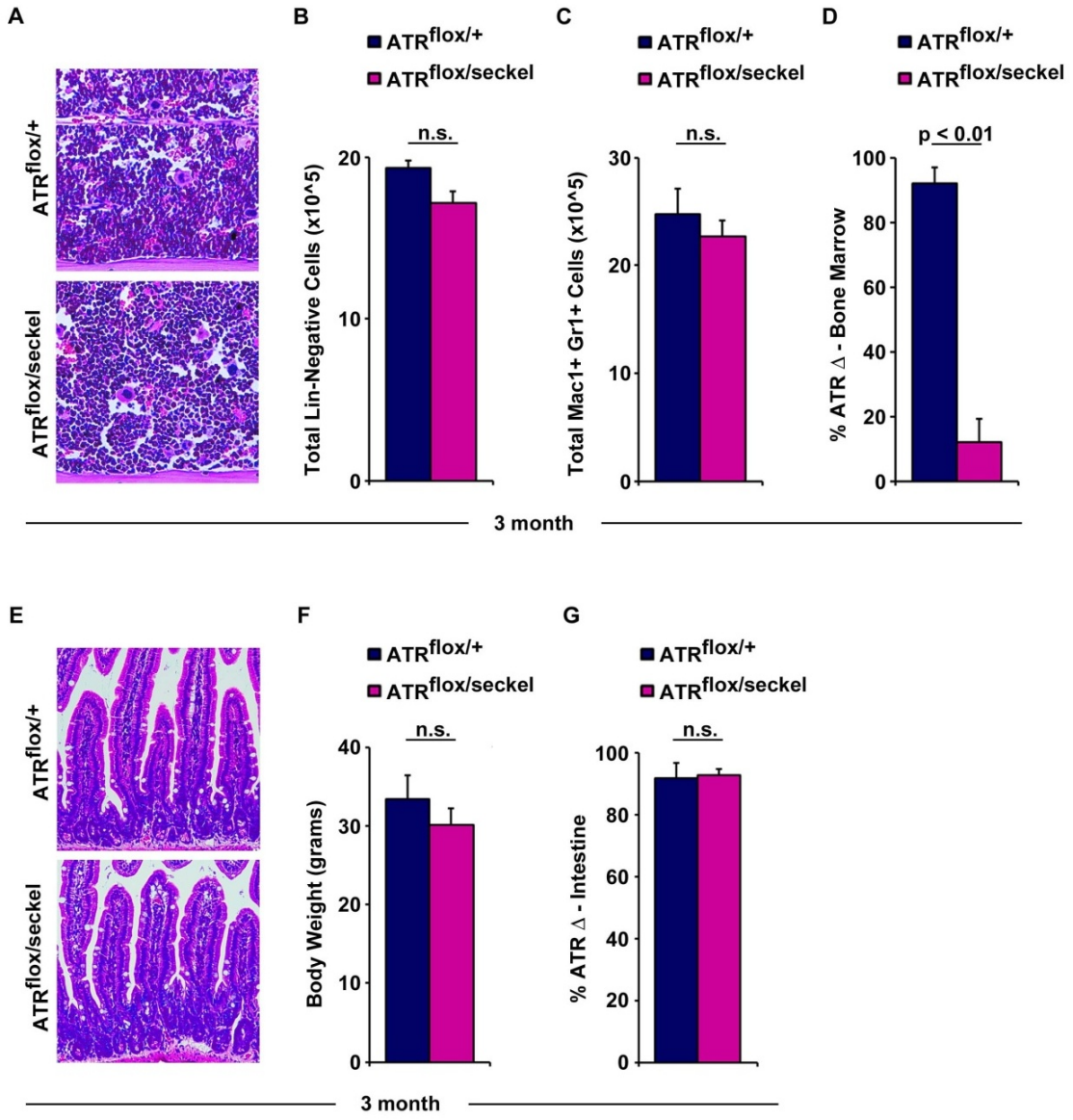

Supplemental Figure 4. ATR suppression does not overtly affect bone marrow or intestinal homeostasis for extended periods of time. (**A**) H&E stained sections of the humeral bone from TAM-treated $ATR^{flox/+}$Cre-$ERT2^{+}$ or $ATR^{flox/seckel}$Cre-$ERT2^{+}$ mice at 3 months after initial treatment, 200X magnification. (**B, C**) Absolute number of lineage-negative bone marrow cells (CD3-negative, B220-negative, Ter119-negative, Mac1-negative) or myeloid cells ($Mac1^{+}$, $Gr1^{+}$) obtained from 4 hindlimb bones of mice at 3 months after initial TAM treatment (n = 2-5 mice per genotype). (**D**) Abundance of the ATR^{flox}-recombined allele (ATR^{Δ}) in the bone marrow of TAM-treated $ATR^{flox/+}$Cre-$ERT2^{+}$ or $ATR^{flox/seckel}$Cre-$ERT2^{+}$ mice at 3 months after initial treatment, as determined through qPCR analysis of genomic DNA isolated from each tissue (n = 3-5 mice per genotype). (**E**) H&E stained sections of intestines from TAM-treated $ATR^{flox/+}$Cre-$ERT2^{+}$ or $ATR^{flox/seckel}$Cre-$ERT2^{+}$ mice at 3 months after initial treatment, 200X magnification. (**F**) Weight of mice at 3 months after initial treatment. (**G**) Abundance of the ATR^{flox}-recombined allele (ATR^{Δ}) in the intestinal epithelium of TAM-treated $ATR^{flox/+}$Cre-$ERT2^{+}$ or $ATR^{flox/seckel}$Cre-$ERT2^{+}$ mice at 3 months after initial treatment.

Supplemental Figure 5

Genotype	Post-Tam	Status at	% Mac1$^+$ Gr1$^+$	Weight	% ATR$^\Delta$ (% ATR-deleted)			
		endpoint	(Marrow)	(grams)	Brain	Marrow	Intestine	Skin
ATR$^{flox/seckel}$ Cre-ERT2$^+$	8 months	Alive, well	57.3	34.8	76.2	-4.6	90.4	92.8
ATR$^{flox/seckel}$ Cre-ERT2$^+$	8 months	Alive, well	58.5	35.1	74.2	-5.5	87.7	82.3
ATR$^{flox/seckel}$Cre-ERT2$^+$	8 months	Alive, well	59.4	41.8	73.1	7.6	78.9	75.8
ATR$^{flox/seckel}$Cre-ERT2$^+$	10 months	Alive, well	71.3	35	81.5	-13.3	83.8	85.2
ATR$^{flox/seckel}$Cre-ERT2$^+$	12 months	Alive, well	76.7	30	82.6	-2.9	89.3	85.7
ATR$^{flox/seckel}$Cre-ERT2$^+$	12 months	Alive, well	66.7	37	75.9	-15.8	86.6	N/A
ATR$^{flox/seckel}$Cre-ERT2$^+$	16 months	Alive, well	50.6	39.7	81.1	1.1	86	93.4
ATR$^{flox/seckel}$Cre-ERT2$^+$	16 months	Alive, well	53.3	38	83.7	1.0	93.9	89.3

Supplemental Figure 5. Analysis of ATR$^{flox/seckel}$Cre-ERT2$^+$ mice at extended time points (8-16 months) following tamoxifen treatment. Determination of Mac1$^+$ Gr1$^+$ and the continued representation of ATR^{flox}-recombined cells over time were performed as described in Methods.

Supplemental Figure 6

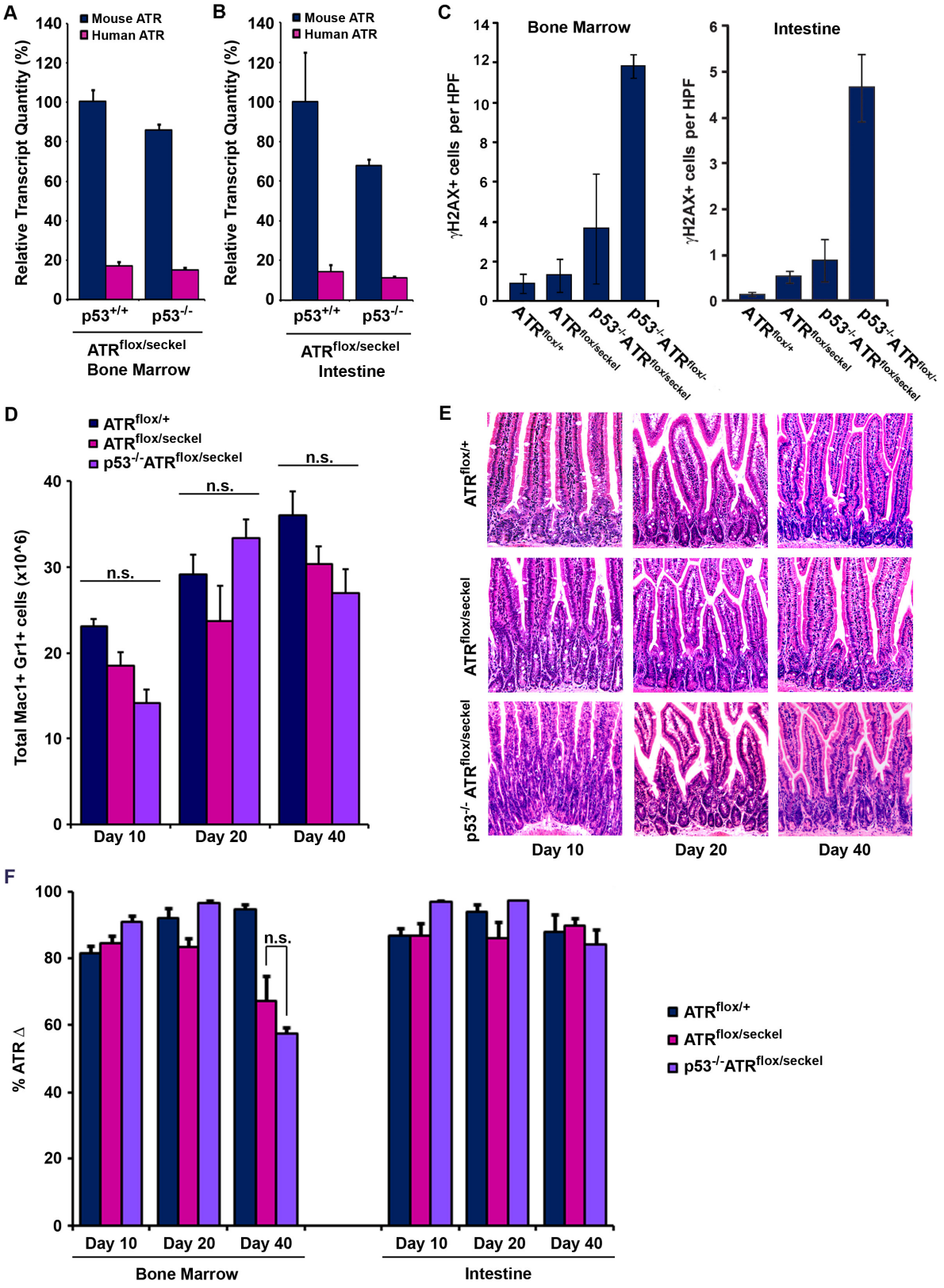

Supplemental Figure 6. ATR suppression is tolerated in p53-deficient mice. (**A,B**) Quantification of correctly-spliced ATR transcript in adult marrow (A) and intestinal epithelium (B); n = 5 mice per genotype, per tissue. (**C**) Number of γH2AX-positive cells in adult tissues 10 days following initiation of TAM treatment. n= 3-5 mice and >10 images (200x) per tissue were quantified. (**D**) Number of $Mac1^{+}$,$Gr1^{+}$ cells from 4 hindlimb bones of mice at the indicated time points after TAM; n = 5-15 mice per genotype, per time point. (**E**) H&E stained sections of intestines from TAM-treated mice, 200X magnification. (**F**) Abundance of the ATR^{flox}-recombined allele (ATR^{Δ}) in the bone marrow (left) and intestines (right) of TAM-treated mice at the indicated time points.

Supplemental Figure 7

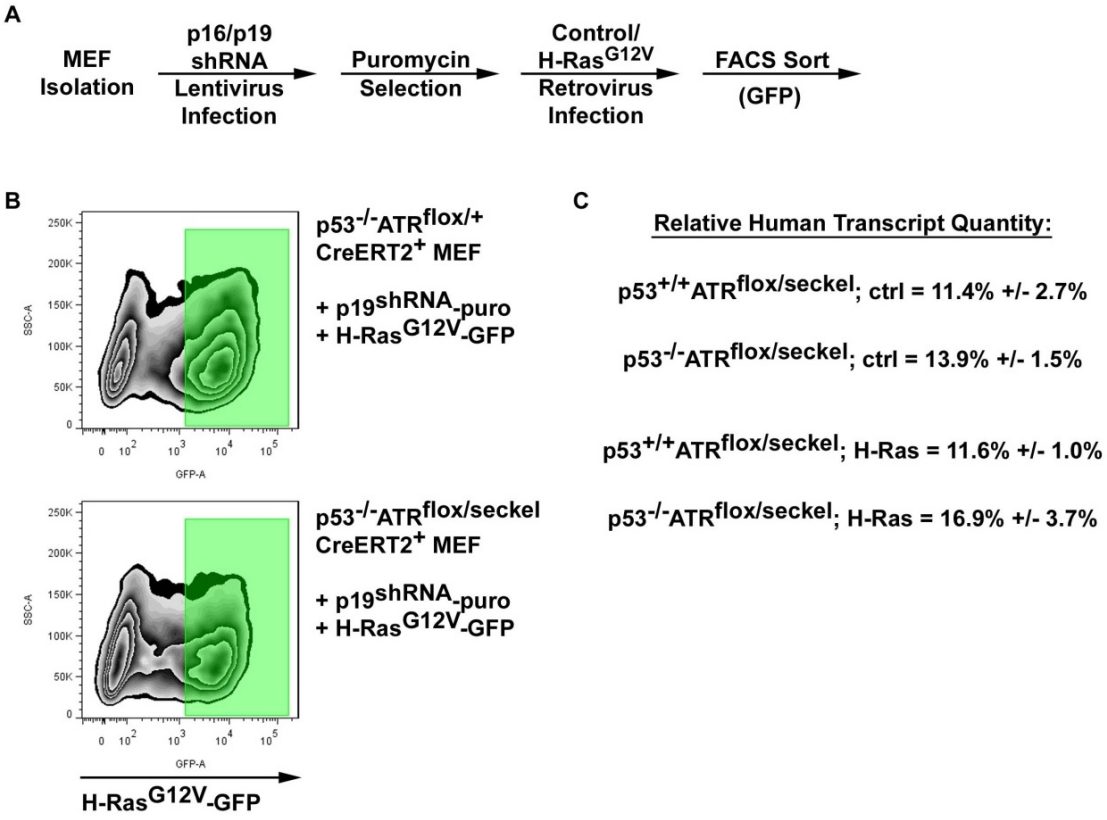

Supplemental Figure 7. Derivation of immortalized/transformed murine embryonic fibroblast (MEF) lines. (**A**) Method used to produce MEF lines used in Figures 4 through 6 of the main text. (**B**) Representative FACS analysis of MEF lines obtained during cell sorting (isolation of GFP+ cells). (**C**) Quantification of correctly-spliced mouse (ATR^{flox}) and human (ATR^{seckel}) ATR transcript in sorted MEF lines.

Supplemental Figure 8

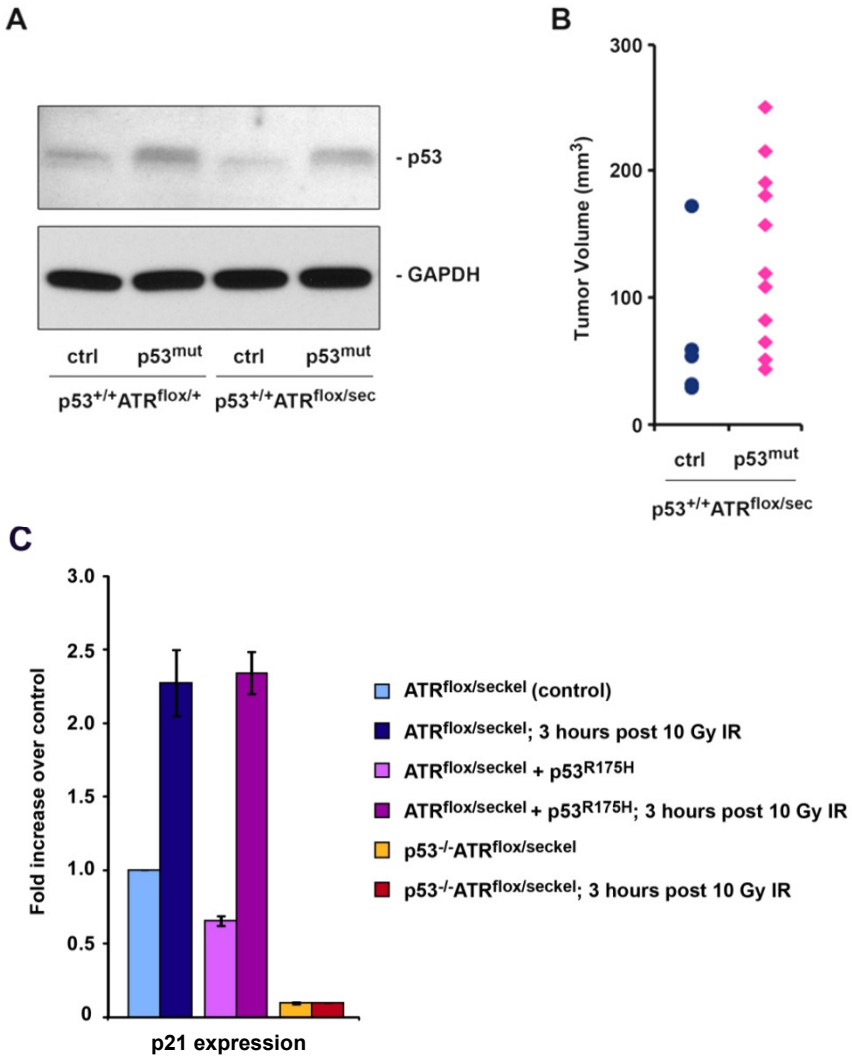

Supplemental Figure 8. Moderate expression levels of $p53^{R175H}$ in $p53^{+/+}ATR^{flox/seckel}$ and control cell lines promotes tumor growth in NCr nude mice but does not inhibit DNA damage-induced transcriptional responses. (**A**) Steady state levels of p53 in cell lines expressing wild-type p53 in the absence (ctrl) or the presence ($p53^{mut}$) of stable ectopic expression of $p53^{R175H}$. Expression of $p53^{R175H}$ was mediated through retrovirus transduction and selection as described in Methods. (**B**) Nude tumor growth of cell lines in **A** following transplantation into NCr nude mice. Each point represents the size individual tumors 8 days after transplantation. Transplantation was performed as described in Figure 4 and Methods. (**C**) DNA damage inducible p53-dependent expression of p21 in $p53^{R175H}$-expressing cells. $ATR^{flox/seckel}$ MEF cells lines (ATR expressing; not TAM treated) were exposed to 10 Gy ionizing radiation. Three hours later, cells were harvested and quantified for p21 mRNA transcript levels by qRT-PCR. Lines expressing the $p53^{R175H}$ mutant in a p53 wild-type background are noted ($p53^{R175H}$). Cell lines that lack p53 expression ($p53^{-/-}$) were used as negative controls. Cell lines used for these experiments are among the same lines utilized in Figures 4, 5 and 6.

Supplemental Figure 9

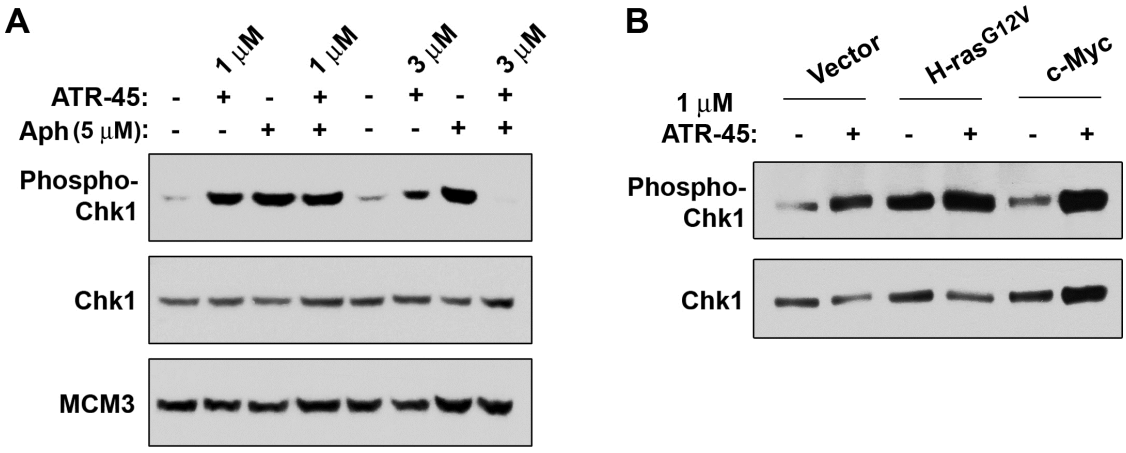

Supplemental Figure 9. Low doses of ATR inhibitor stimulate Chk1-S345 phosphorylation. (**A**) Asynchronous passage-immortalized murine fibroblasts were treated with ATR-45 inhibitor or 5 μM aphidicolin for 6 hours. The inhibitory effects of 3 μM ATR-45 were readily observed under the saturating levels of replication stress produced by 5 μM aphidicolin treatment. In contrast, 1 μM ATR-45 stimulated Chk1 phosphorylation in the absence of aphidicolin treatment. (**B**) The stimulatory effects of 1 μM ATR-45 inhibitor (6 hours treatment) on Chk1 phosphorylation were also observed in NIH3T3 stable cell lines (Figure 7 and 8) transduced with empty vector, H-ras^{G12V} or c-Myc-expressing retrovirus. Samples in **A** and **B** were normalized for total protein prior to loading.

Supplemental References

1. Meyers EN, Lewandoski M, Martin GR. An Fgf8 mutant allelic series generated by Cre- and Flp-mediated recombination. *Nat Genet*. 1998;18:136–141.

2. Nagy A, et al. Dissecting the role of N-myc in development using a single targeting vector to generate a series of alleles. *Curr Biol*. 1998;8:661–664.

3. Levin SI, Meisler MH. Floxed allele for conditional inactivation of the voltage-gated sodium channel Scn8a (NaV1.6). *Genesis*. 2004;39:234–239

4. Ragland RL, Arlt MF, Hughes ED, Saunders TL, Glover TW. Mice hypomorphic for Atr have increased DNA damage and abnormal checkpoint response. *Mamm Genome*. 2009; 20(6):375-85.

Supplemental Methods

Quantitative RT-PCR. RNA was isolated through a TRIzol (Invitrogen) extraction, followed by further purification through an RNeasy Mini Kit (Qiagen) according to manufacturer's instructions. cDNA was produced with a High Capacity cDNA Reverse Transcription Kit (Applied Biosystems) according to manufacturer's instructions. cDNA was then serially diluted and used in quantitative RT-PCR reactions with assays designed to detect either correctly spliced (e.g. containing exon 9) mouse ATR or human ATR, as described in Figure S2. All reactions were performed in triplicate for each sample with TaqMan Universal PCR Master Mix (Applied Biosystems) on the Applied Biosystems 7900HT Sequence Detection System.

Histological Analysis. Tissues were fixed in 4% paraformaldehyde (PFA) at 4^{o}C overnight, dehydrated, and embedded in paraffin. For histological examination, tissues were sectioned and stained with hematoxylin and eosin (H&E) or specific antibodies. γH2AX was detected by immunofluorescence with mouse anti-phospho-H2AX (Ser139)-FITC conjugated antibodies (1:50 dilution, Millipore 16-202A).

Bone marrow (FACS) analysis. Bone marrow was isolated from 4 hindlimb bones by flushing into cold media and filtering through a nylon mesh strainer. RBCs were lysed using ACK Lysing Buffer (Lonza), and cells were counted with a Coulter Counter (Becton Dickson). Conjugated antibodies used for staining included: Mac1/CD11b-APC (M1/70), Gr1/Ly-6G-PE (8C5), CD3-FITC (2C11), B220-FITC (6B2), and TER119-FITC (TER-119). All antibodies were obtained from eBiosciences. Dead cells were excluded with 7-AAD, cell analysis was performed on a FACSCalibur (Becton Dickson), and data was analyzed using FlowJo version 4.6.2 (Tree Star).

Quantitative PCR. Genomic DNA was isolated from tissues using a DNeasy Blood and Tissue Kit (Qiagen) as per manufacturer's instructions. DNA was diluted to a concentration of 2ng/μl in nuclease-free water and used directly in subsequent PCR reactions. Sequence-specific primers and probes targeting the conditional

region of the ATR^{flox} gene were designed using Primer Express (Applied Biosystems). Primer/probe sequences were:

ATR^{flox} forward primer: 5'- CCGCTCGCTCGGTTTAAA

ATR^{flox} reverse primer: 5'- TCCCCGCATGCAAGCTT

ATR^{flox} probe: 5'- 6FAM-TCATAACTTCGTATAGCATACA

Mouse GAPD (Applied Biosystems) was purchased as a pre-developed TaqMan assay and used as an endogenous control in ΔΔCT analysis. PCR reactions were performed in a final volume of 20µl using TaqMan Universal PCR Master Mix (Applied Biosystems), 8ng of genomic DNA, 0.9µM of each primer and 0.25µM of probe. All reactions were carried out in triplicate for each sample and performed on the Applied Biosystems 7900HT Sequence Detection System.

Quantification of S-phase content/apoptosis. Cells were treated with 10µM EdU (Invitrogen), collected 30 minutes later, and fixed in 70% ethanol. EdU incorporation was detected with a Click-iT EdU Alexa Fluor 647 Assay Kit (Invitrogen). For detection of apoptosis, cells were collected, resuspended to a final concentration of $1x10^6$ cells per mL in 1X binding buffer (0.1M Hepes, 1.4M NaCl, 25 mM CaCl2, pH 7.4) and stained with Annexin V-APC and 7-AAD (BD Pharmingen) according to manufacturer's instructions. Cell analysis was performed on a FACSCalibur (Becton Dickson).